Research Article

Advances in Mechanical Engineering

Advances in Mechanical Engineering
2016, Vol. 8(7) 1–12

DOI: 10.1177/1687814016656108
aime.sagepub.com
SAGE

High mechanical advantage design of six-bar Stephenson mechanism for servo mechanical presses

Jianguo Hu[1,2], Yousong Sun[2] and Yongqi Cheng[2]

Abstract

This article proposed a two-phase design scheme of Stephenson six-bar working mechanisms for servo mechanical presses with high mechanical advantage. In the qualitative design phase, first, a Stephenson six-bar mechanism with a slide was derived from Stephenson six-bar kinematic chains. Second, based on the instant center analysis method, the relationship between mechanical advantage and some special instant centers was founded, and accordingly a primary mechanism configuration with high mechanical advantage was designed qualitatively. Then, a parameterized prototype model was established, and the influences of design parameters toward slide kinematical characteristics were analyzed. In the quantitative design phase, a multi-objective optimization model, aiming at high mechanical advantage and dwelling characteristics, was built, and a case design was done to find optimal dimensions. Finally, simulations based on the software ADAMS were conducted to compare the transmission characteristics of the optimized working mechanism with that of slide-crank mechanism and symmetrical toggle mechanism, and an experimental press was made to validate the design scheme. The simulation and experiment results show that, compared with general working mechanisms, the Stephenson six-bar working mechanism has higher mechanical advantage and better dwelling characteristics, reducing capacities and costs of servo motors effectively.

Keywords

Servo mechanical press, working mechanism, instant center, mechanical advantage, optimum design

Date received: 26 January 2016; accepted: 31 May 2016

Academic Editor: Yangmin Li

Introduction

Servo mechanical presses are novel metal forming equipments utilizing servo drive technology. They can offer the flexibility of hydraulic presses and productivity of mechanical presses, being propitious to improve the forming limit, product accuracy, and working environment.[1]

The most common working mechanism for traditional mechanical presses is the slide-crank mechanism (SCM) with a heavy flywheel mounted on the high-speed shaft. The flywheel, accumulating the mechanical energy during empty stroke and releasing the stored energy during forming, can reduce the capacity and restrain the speed variation of the induction motor (IM). The flywheel, however, is disadvantageous for servo mechanical presses, which pursue low inertia because of the increasing demands on the flexibility of

[1]Faculty of Mechanical & Electrical Engineering, Shunde Polytechnic, Foshan, China
[2]Faculty of Materials and Energy, Guangdong University of Technology, Guangzhou, China

Corresponding author:
Jianguo Hu, Faculty of Mechanical & Electrical Engineering, Shunde Polytechnic, Desheng East Road, Shunde District, Foshan City 528300, Guangdong Province, China.
Email: jghu-sd@139.com

slide motion. Therefore, for most servo mechanical presses, flywheels have to be removed and the forming forces are supplied totally by servo motors (usually, permanent magnet synchronous motors (PMSMs)). Hence, when common SCMs with low mechnical advantage are adopted as working mechanisms of servo presses, the capacities of PMSMs would have to been increased greatly, which raising manufacturing costs and hindering development and popularity of servo mechanical presses, especially the large-tonnage ones.

Generally, mechanical transmission system of servo mechanical presses includes driving elements, reducing mechanisms, and working mechanisms. In order to develop mechanical servo presses with large tonnage and low costs, several approaches are studied to develop new driving technologies or transmission mechanisms.

One of them is to develop hybrid driving technology, in which a large IM with constant speed and a small PMSM with variable speed were integrated together. The output motions from the IM and PMSM were synthesized by a 2 degree-of-freedom hybrid drive mechanism. Du and Guo,[2] Meng et al.,[3] Li and Zhang,[4] Guo et al.,[5] and Ouyang et al.[6] conducted the studies on a 7R-type seven-bar linkage. He et al.,[7,8] Tang and Guo,[9] and Soong[10] conducted the studies on a 5R2P-type seven-bar linkage. Li et al.[11] and Tso and Liang[12] conducted the studies on a nine-bar linkage. Tokuz and Jones[13] and Wang et al.[14] conducted the studies on a differential gearbox.

Another approach is to develop novel transmission mechanisms to cut down the capacities of PMSMs. Guo and colleagues[15–17] proposed a parallel kinematic mechanism (PKM)-type transmission mechanism based on a parallel mechanism and a dual screw transmission mechanism. Sun et al.[18] and Suzuki and Hata[19] adopted double reducing mechanisms to increase reduction ratio.

In the former case, the hybrid driving technology combines advantages of the inexpensive IM and flexible PMSM; however, the uncontrollability of the IM makes it difficult for the slide to stop or turn around in the approaching stroke, which are demanded by some sheet metal forming technologies, such as blending, coining, deep drawing, hot stamping, and so on, introduced by Osakada et al.[1] Moreover, due to the dynamic interaction of the two motors of different types, they have to counteract in power to obtain some required slide motion trajectories.

In the latter case, the adoption of parallel mechanisms will not cut down the total required capacities of PMSMs, but increasing the complexity for synchronization control. And too high reduction ratio will decrease the production efficiency of mechanical presses to an unacceptable degree, because the rated speed of large capacity servo motor is usually just a few hundred rotations per minute.

This article focuses on the development of Stephenson six-bar mechanisms (SSMs) with high mechanical advantage to cut down the capacities of servo motors. First, an instant center analysis method was presented to design qualitatively the primary mechanism configuration with high mechanical advantage, and then, a multi-objective optimization method was employed to synthesize the dimensions of the mechanism. Instant center analysis method has been successfully applied to the design of automobile rear suspension systems[20] and optical adjusting mechanisms,[21] proven to be a visual, qualitative analysis technology. While, the multi-objective optimization design method is an analytic, quantitative technology. Hwang et al.[22] employed a multi-objective optimization method to synthesize the drag-link of mechanical press for precision drawing. In that case, the objective functions include the maximum normal force on the guide, mean mechanical advantage, variance of the drawing speed, and so on. In order to optimize the balancing design of the drag-link drive with adding disk counterweights, Chiou et al.[23] used a multi-objective optimization method to minimize the fluctuations of the shaking force and shaking moment. Smaili and Diab[24] applied an ant-gradient algorithm to solve the multi-objective dimensional synthesis problem of planar four-bar mechanisms, by considering transmission angle and mechanical advantage constraint into the objective function.

The purpose of this study is to propose a two-phase design scheme, qualitative and quantitative, to obtain a Stephenson six-bar working mechanism with high mechanical advantage for 1 degree-of-freedom servo mechanical presses, reducing the required PMSM capacity and improving the controllability, without decreasing the production efficiency. In the qualitative design phase, the relationship between mechanical advantage and instant centers is built and used to find the mechanism configuration with high mechanical advantage. While in the quantitative design phase, a multi-objective optimization model, with mechanical advantage, low-speed characteristics, and slow-moving uniformity of the slide being considered into objective functions, is constructed and solved. And some simulation and experiment studies were done to validate the design results.

Stephenson six-bar working mechanism

The six-bar linkage of four binary bars and two ternary bars has two valid isomers, Watt's chain and Stephenson's chain.[18] The six bars and seven joints of the Stephenson six-bar linkage compose one four-bar

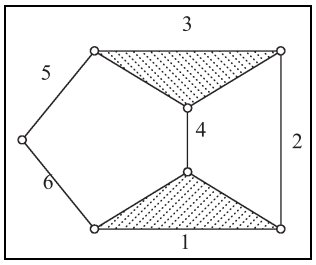

Figure 1. Stephenson six-bar kinematic chain.

loop and one five-bar loop. It has two ternary links that are separated by a binary link, as shown in Figure 1. Once link 1 is chosen as the frame, link 2 as the input crank, and the revolute pair between links 6 and 1 is evolved into a sliding pair, a Stephenson-type six-bar mechanism with a slide can be derived, as shown in Figure 2. The continuous rotation of input crank 2 can be converted into a reciprocation of slide 6, which can be used as a working mechanism for servo mechanical presses. It should be noted that, being different from the conventional toggle mechanism, the connecting rod 3 of the SSM is a ternary link, which will bring about different transmission characteristics.

Qualitative design based on instant centers

Relationship between mechanical advantage and instant centers

The mechanical advantage of a mechanism could be defined as the ratio of the output force or torque to the input one.[20] In order to cut down the capacities of servo motors, the mechanical advantage within the slide working stroke should be as high as possible. For the SSM with a slide, the main output is the forming force applied to the slide, and the input refers to the input torque applied to the crank.

According to the definition of instant center of rotation, at a particular instant of time, there is a coincidence point with the same speed for the input part and output part of a linkage mechanism undergoing planar movement, and thus, the following relationship can be achieved

$$\omega_i \cdot \overline{I_{1i}I_{io}} = \omega_o \cdot \overline{I_{1o}I_{io}} \tag{1}$$

where ω_i denotes the angular speed of input part, ω_o is the angular speed of output part, I_{1i} is the instant center between input part and frame, I_{1o} is the instant center between output part and frame, I_{io} is the instant center between input part and output part, $\overline{I_{1i}I_{io}}$ is the distance of instant centers between I_{1i} and I_{io}, and $\overline{I_{1o}I_{io}}$ is the distance of instant centers between I_{1o} and I_{io}.

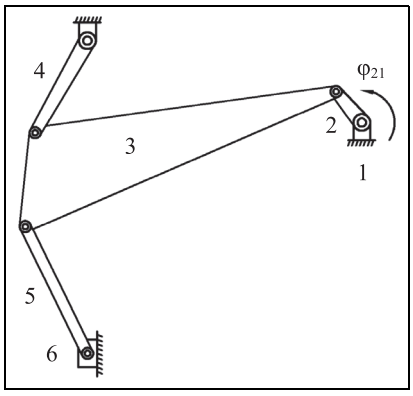

Figure 2. Stephenson six-bar mechanism with a slide.

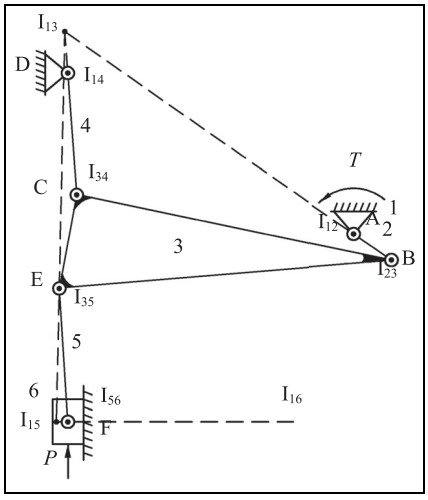

Figure 3. Stephenson six-bar mechanism with a slide.

Figure 3 shows the locations of some special instant centers when the working mechanism is at working stroke.

Assuming the friction and inertia are ignored, according to the principle of virtual work, for the SSM with a slide, the following relationship can be found

$$T_i \cdot \omega_i = F_o \cdot v_o \tag{2}$$

where F_o denotes the forming force, T_i is the input torque, ω_i is the angular speed of the crank, and v_o is the linear speed of the slide.

Note that the slide is evolved from link 6, the relationship between the linear speed of the slide and the angular speed of the link 6 can be written as follows

$$v_o = \overline{I_{56}I_{16}} \cdot \omega_o \tag{3}$$

Based on equations (1)–(3), the mechanical advantage of the SSM can be defined as follows

Table 1. Relationship between the limit value of MA^* and the location features of instant centers.

Case		Mechanical advantage	Location features of instant centers
1	Num → zero	Zero	I_{13} is coincident with I_{23} or/and I_{15} is coincident with I_{35}
2	Den → infinity	Zero	Never happen
3	Num → infinity	Infinity	Never happen
4	Den → zero	Infinity	I_{13} is coincident with I_{35} or/and I_{15} is coincident with I_{56}

$$MA = \frac{F_o}{T_i} = \frac{\omega_i}{v_o} = \frac{\overline{I_{1o}I_{io}}}{\overline{I_{56}I_{16}} \cdot \overline{I_{1i}I_{io}}} = \frac{\overline{I_{16}I_{26}}}{\overline{I_{56}I_{16}} \cdot \overline{I_{12}I_{26}}} \quad (4)$$

By the Aronhold-Kennedy theorem and geometric principle, equation (5) can be obtained

$$\frac{\overline{I_{16}I_{26}}}{\overline{I_{12}I_{26}}} = \frac{\overline{I_{16}I_{26}} \cdot \overline{I_{35}I_{15}} \cdot \overline{I_{23}I_{13}}}{\overline{I_{15}I_{56}} \cdot \overline{I_{35}I_{13}} \cdot \overline{I_{23}I_{12}}} \quad (5)$$

Note that the instant center I_{16} is at infinity, equation (6) can be written as follows

$$\frac{\overline{I_{16}I_{26}}}{\overline{I_{56}I_{16}}} = 1 \quad (6)$$

By substituting equations (5) and (6) into equation (4), the mechanical advantage can be rewritten as follows

$$MA^* = \frac{\overline{I_{35}I_{15}} \cdot \overline{I_{23}I_{13}}}{\overline{I_{15}I_{56}} \cdot \overline{I_{35}I_{13}} \cdot \overline{I_{23}I_{12}}} \quad (7)$$

It is noted that the mechanical advantage of the Stephenson six-bar working mechanism is associated with the locations of the six instant centers I_{12}, I_{23}, I_{35}, I_{56}, I_{13}, and I_{15}. According to equation (7), there are four cases that will make MA^* to go to the limit value, namely zero or infinity, as shown in Table 1. When the numerator goes to zero and denominator does not (case 1), or when the denominator goes to infinity and numerator does not (case 2), MA^* will go to zero. When the numerator goes to infinity and denominator does not (case 3), or when the denominator goes to zero and numerator does not (case 4), MA^* will go to infinity.

In this study, the known instant centers, such as I_{12}, I_{23}, I_{35}, and I_{56}, are referred to as the primary instant centers. The unknown instant centers, such as I_{13} and I_{15}, are referred to as the secondary instant centers. Compared with the central-in-space primary instant centers, the secondary instant centers are widely distributed in the domain, which have significant impacts to the mechanical advantage.

Based on equation (7), the following analytic results can be given:

1. The distance of instant centers $\overline{I_{23}I_{12}}$ refers to the length of the input crank, so its value will never go to zero or infinity. When the secondary instant centers I_{13} and/or I_{15} are at infinity, both the numerator and denominator will go to infinity. Therefore, it could be said that case 2 and case 3 will never happen.
2. When the secondary instant center I_{13} is coincident with the primary instant center I_{23}, or/and the secondary instant center I_{15} is coincident with the primary instant center I_{35}, the numerator will go to zero, and then case 1 will happen.
3. When the secondary instant center I_{13} is coincident with the primary instant center I_{35}, or/and the secondary instant center I_{15} is coincident with the primary instant center I_{56}, the denominator will go to zero, and then case 4 will happen.

Special primary mechanism configuration with high mechanical advantage

In order to obtain high mechanical advantage within working stroke, it is necessary to ensure that the numerator of the fraction in equation (7) is as large as possible, while the denominator as small as possible. Based on this, some suggestions for qualitative design of the primary mechanism configuration with high mechanical advantage can be listed as follows:

1. Note that the denominator of the fraction in equation (7) is the product of distances of instant centers $\overline{I_{15}I_{56}}$, $\overline{I_{35}I_{13}}$, and $\overline{I_{23}I_{12}}$. The mechanical advantage is tightly associated with $\overline{I_{15}I_{56}}$ and $\overline{I_{35}I_{13}}$. When the crank rotates from the nominal position (the beginning of working stroke) to the bottom dead center (BDC; the end of working stroke), if I_{13} and I_{15} are, respectively, approaching to I_{35} and I_{56}, the high mechanical advantage can be obtained. This can be ensured by adjusting the locations of primary instant centers I_{34}, I_{35}, and the orientation of link 2, as shown in Figure 3. Namely, the instant center I_{34} (or I_{35}) should be a little to the left (or right) from the vertical line between points D and F, and the instant center I_{23} should lie in the lower right of I_{12}.
2. Note that the numerator of the fraction in equation (7) is the product of $\overline{I_{23}I_{13}}$ and $\overline{I_{35}I_{15}}$, so the mechanical advantage can be improved by

Table 2. Relationship between the design parameters and the kinematic dimensions.

Design parameters	x_1	x_2	x_3	x_4	x_5	x_6	x_7	x_8	x_9	x_{10}
Kinematic dimensions	$\vec{l}_1$	$\vec{l}_2$	$\vec{l}_3$	$\vec{l}_4$	$\vec{l}_6$	ϕ_{11}	ϕ_{21}	ϕ_{31}	γ	ϕ_{61}

Table 3. Relationship between the design parameters and the kinematic dimensions.

Points	X-coordinate values	Y-coordinate values
A	0	0
B	$x_2 * \cos x_7$	$x_2 * \sin x_7$
C	$x_2 * \cos x_7 + x_3 * \cos x_8$	$x_2 * \sin x_7 + x_3 * \sin x_8$
D	$x_1 * \cos x_6$	$x_1 * \sin x_6$
E	$x_2 * \cos x_7 + x_4 * \cos(x_8 + x_9)$	$x_2 * \sin x_7 + x_4 * \sin(x_8 + x_9)$
F	$x_1 * \cos x_6$	$x_2 * \sin x_7 + x_4 * \sin(x_8 + x_9) + x_5 * \sin x_{10}$

increasing the length of link 3 and link 5, unless the frame is unallowable.

3. The distance of instant centers $\overline{I_{23}I_{12}}$ is the length of the crank, having some influence to the mechanical advantage but a lot to the slide maximum stroke. Thus, the smaller of the crank length, the larger of the mechanical advantage, but restrained by the constraint of slide maximum stroke.

Based on above suggestions, a mechanism configuration with high mechanical advantage, as shown in Figure 3, can be sketched by qualitative design, which is advantageous to reduce the searching domain of design variables and to simplify the numeric computation of optimization model.

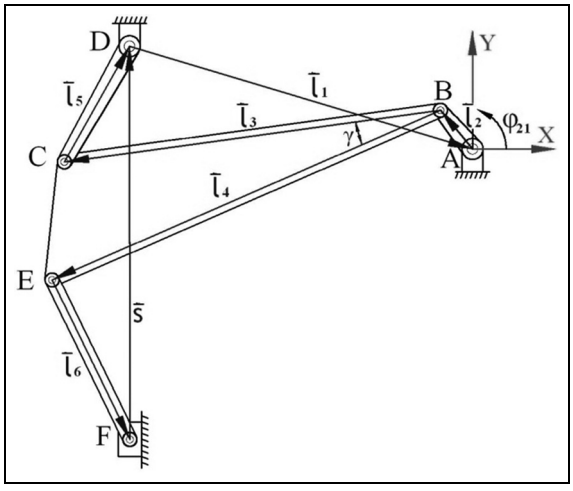

Figure 4. The parameterized configuration of the six-bar working mechanism.

Kinematic design study

Figure 3 is just a primary mechanism configuration designed qualitatively from the view of mechanical advantage. It is also necessary to study its kinematic characteristics, such as the slide maximum stroke, the slide speed monotonic property, and so on. The slide maximum stroke is an important performance index, deciding the working capability of mechanical presses. The slide speed monotonic property means that when the crank keeps unidirectional rotation and the slide is approaching from the top dead center (TDC) to the BDC, the motion direction of the slide always keeps downward, without turning around.

The purpose of kinematic design study is to analyze the sensitivities of design parameters to the slide maximum stroke and slide speed monotonic property. Using vector loop method, the mechanism configuration designed in section "Qualitative design based on instant centers" can be defined by 6 points A, B, C, D, E, and F, and parameterized by 10 variables, as shown in Figure 4. The coordinate values of the six points can be parameterized by the norms of vectors $\vec{l}_1$, $\vec{l}_2$, $\vec{l}_3$, $\vec{l}_4$, $\vec{l}_6$ and the related orientations ϕ_{11}, ϕ_{21}, ϕ_{31}, γ, and ϕ_{61}. The 10 design dimensions can be set as the design parameters x_j $(j = 1 - 10)$, respectively, as shown in Table 2. The coordinate values of the six points can be given by the design parameters, as shown in Table 3.

Based on software MSC/ADAMS, the kinematic design study was conducted to analyze the influences of design parameters toward the slide maximum stroke and the speed monotonic property. Figure 5(a)–(d) shows, respectively, the influences of $\vec{l}_1$, $\vec{l}_2$, $\vec{l}_3$, and $\vec{l}_4$ toward those kinematic characteristics, where curve A denotes the border line of the slide maximum stroke. The arrowhead side is the zone (caller A zone) that the slide maximum stroke is greater than 200 mm. Curve B denotes the border line of the slide speed monotonic property. The arrowhead side is the zone (caller B

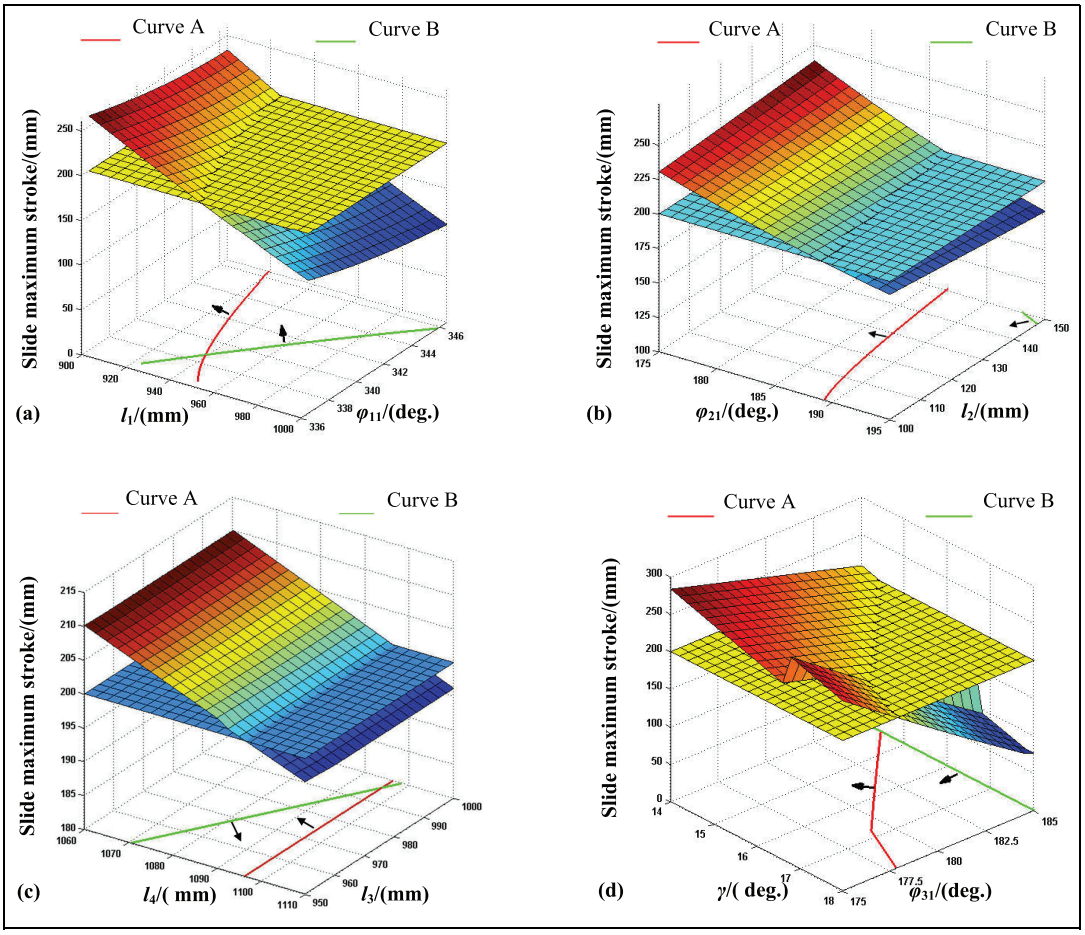

Figure 5. Influences of design parameters toward slide maximum stroke and speed: (a) $x1$ and $x6$; (b) x_2 and x_7; (c) x_3 and x_4 and (d) x_8 and x_9.

zone) that the slide speed is monotonic. The intersection of A zone and B zone is the effective zone that meets the kinematic requirements of enough slide maximum stroke and monotonic slide approaching direction. The results of kinematic design study are useful for the optimization model to decide appropriate initial values and value ranges of the design parameters in section "Multi-objective optimum design."

Multi-objective optimum design

Multi-objective function

Besides the high mechanical advantage, the other requirements for servo mechanical presses are low-speed characteristics and slow-moving uniformity within the working stroke, namely dwelling characteristics, which is beneficial to reduce the speed-changing requirement within slide approaching stroke.[25] Thus, the optimum design here is a multi-objective problem.

It is assumed that the forming force applied to the slide is constant, and the torque required to apply to the input crank can be measured by building measure functions in the software MSC/ADAMS, the non-dimensionalized mechanical advantage can be expressed as follows

$$f_1(x_j) = \frac{T_{ref}}{T(t)} \quad (j = 1 - 10) \tag{8}$$

where x_j $(j = 1 - 10)$ denote the design variables of the optimization model, $T(t)$ is the value of measure function used to measure the crank torque within working stroke, and T_{ref} is the constant reference value of the crank torque.

The low-speed characteristics can be expressed by the relative average speed of the slide within working stroke as follows

$$f_2(x_j) = \frac{\bar{V}}{V_{ref}} \quad (j = 1 - 10) \tag{9}$$

The slow-moving uniformity can be expressed in terms of coefficient of standard deviation of the slide speed within working stroke as follows

$$f_3(x_j) = \sqrt{\left[\sum_{i=1}^{N}(V_i - V)^2\right] \Big/ N} \Big/ \bar{V} \quad (j = 1 - 10) \quad (10)$$

where V_i (mm/s) is the value of slide speed within working stroke, $\bar{V}$ (mm/s) is the average value of slide speed, and N is the number of sampling data.

In this study, it is aimed at maximizing the mechanical advantage and minimizing the slide's average speed and speed uniformity within the working stroke. For the multi-objective problem, the following multi-objective function is constructed

$$\text{Minimize } f(x_j) = \frac{\omega_1}{f_1} + \omega_2 f_2 + \omega_3 f_3 \quad (j = 1 - 10) \quad (11)$$

where ω_1, ω_2, and ω_3 are the weighting factors, given as percentage values, such as 70%, 20%, and 10%, respectively.

Design variables

The kinematic dimensions, as shown in Table 2, are set as the design variables x_j $(j = 1 - 10)$ for optimization. The initial values of the design variables can be given based on the suggestions for qualitative design of primary mechanism configuration in section "Qualitative design based on instant centers."

Constraints

The constraints of the optimization model are mainly dominated by the space limitation and performance requirements of the working mechanism. The space limitation includes the bond values of the design variables and the allowable maximum swag angles of link 4 and link 5. The performance requirements include the desired slide maximum stroke and the slide speed monotonic property. The constraints about allowable maximum swag angles and slide maximum stroke can be decided by the performance index. The constraints about the bond values of design variables and slide speed monotonic property can be given in the light of results of kinematic design study in section "Kinematic design study." Based on this, the constraints can be expressed as follows

$$\begin{aligned} &\text{Subject to} \\ &g_j = x_{jl} \leqslant x_j \leqslant x_{ju} \quad (j = 1{-}10) \\ &g_{11} = 0 \leqslant \alpha \leqslant \alpha_u \\ &g_{12} = 0 \leqslant \beta \leqslant \beta_u \\ &g_{13} = S_{\max l} \leqslant \text{Max}(S) \leqslant S_{\max u} \\ &g_{14} = V_{\text{sign}} \leqslant 0 \end{aligned} \quad (12)$$

where x_{jl} and x_{ju} are, respectively, the lower bound and upper bound of the design variables x_j; α and β are measure functions for swag angles of link 4 and link 5, respectively; α_u and β_u are allowable maximum swag angles of link 4 and link 5, respectively; Max(S) is the function used to get the maximum value of slide stroke. $S_{\max l}$ and $S_{\max u}$ are the required minimum and maximum values of slide stroke, respectively; V_{sign} is the sign function used to identify the direction of the slide motion within approaching stroke (from the TDC to the BDC), and the negative value means that the slide is moving to the BDC.

It can be found that the optimization is a nonlinear constrained optimization problem, and it can be solved by the embedded algorithm, namely, Sequential Quadratic Programming.

Case design and comparative analysis

The performance requirements of a working mechanism are given as shown in Table 4, where the nominal pressure is the reference value about mechanical presses' tonnage, the slide maximum stroke is the stroke range between the TDC and BDC, and the nominal pressure stroke means the slide stroke range able to undergo the nominal pressure. The initial values of the design variables are given as shown in Table 5. The design constrains are assigned as shown in Table 6. Based on the multi-objective optimization model in section "Multi-objective optimum design" and the

Table 4. Performance requirements for all working mechanisms.

Performance requirements	Nominal pressure	Slide maximum stroke	Nominal pressure stroke	Default stroke rate
Values/units	4000/kN	200/mm	6/mm	30/spm

Table 5. Initial values of the design variables of the SSM.

Design variables	x_1	x_2	x_3	x_4	x_5	x_6	x_7	x_8	x_9	x_{10}
Initial values	920	125	970	1085	450	340	185	180	16	310

SSM: Stephenson six-bar mechanism.

Table 6. Design constrains of the SSM.

$g_1 = 900 \leqslant x_1 \leqslant 940$ mm	$g_8 = 175 \leqslant x_8 \leqslant 185^\circ$
$g_2 = 100 \leqslant x_2 \leqslant 150$ mm	$g_9 = 14 \leqslant x_9 \leqslant 18^\circ$
$g_3 = 950 \leqslant x_3 \leqslant 995$ mm	$g_{10} = 305 \leqslant x_{10} \leqslant 315^\circ$
$g_4 = 1070 \leqslant x_4 \leqslant 1098$ mm	$g_{11} = 0 \leqslant$ Mea_USwagAng $\leqslant 50^\circ$
$g_5 = 400 \leqslant x_5 \leqslant 490$ mm	$g_{12} = 0 \leqslant$ Mea_BSwagAng $\leqslant 50^\circ$
$g_6 = 336 \leqslant x_6 \leqslant 346^\circ$	$g_{13} = 200 \leqslant$ Max(Fun_Stroke) $\leqslant 210$ mm
$g_7 = 175 \leqslant x_7 \leqslant 190^\circ$	$g_{14} =$ Fun_Slide velocity < 0

SSM: Stephenson six-bar mechanism.

Table 7. Optimum values of the design variables of the SSM.

Design variables	x_1	x_2	x_3	x_4	x_5	x_6	x_7	x_8	x_9	x_{10}
Optimum values	930.5	135.0	983	1096	465	341.5	188	180	16	311
Objective function	T	T_{ref}	$\bar{V}$	$\bar{V}_{ref}$	f_1	f_2	f_3	f		
Objective function values	41,882	200,000	16	60	4.78	3.75	3.80	5.32		

SSM: Stephenson six-bar mechanism.

software MSC/ADAMS, the optimized values of the design variables and the corresponding multi-objective function value are solved, as shown in Table 7.

In order to compare the transmission characteristics of the optimum SSM with that of general working mechanisms, such as SCM and symmetrical toggle mechanism (STM), the three working mechanisms with the same performance requirements (as shown in Table 4) have been modeled and simulated by the software MSC/ADAMS.

Figure 6(a) and (b) is the structure diagrams of the SCM and STM, respectively. The information about rod length, rod mass, and friction coefficient are shown in Table 8.

Figure 7 is the virtual prototype of the SSM according to the optimum values of rod dimensions in Table 7. Here, several hypotheses were made as follows:

1. All parts are rigid;
2. All clearances at joints are ignored;
3. The material property of all parts is steel, which decides the mass of rods and slide;
4. The radius of pins in all joints is 85 mm;
5. The static and dynamic friction factors of all joints are 0.05;
6. The servo motor runs at a constant speed without speed volatility.

Based on the same calculation conditions, such as the same input speed of crank pi rad/s, end time of 2 s and step size of 0.01 s, the simulations of the three working mechanisms for servo mechanical presses were conducted and some comparison results were got, including slide stroke curves, slide speed curves, crank torque curves, and allowable load curves, as shown in Figures 8–11, respectively.

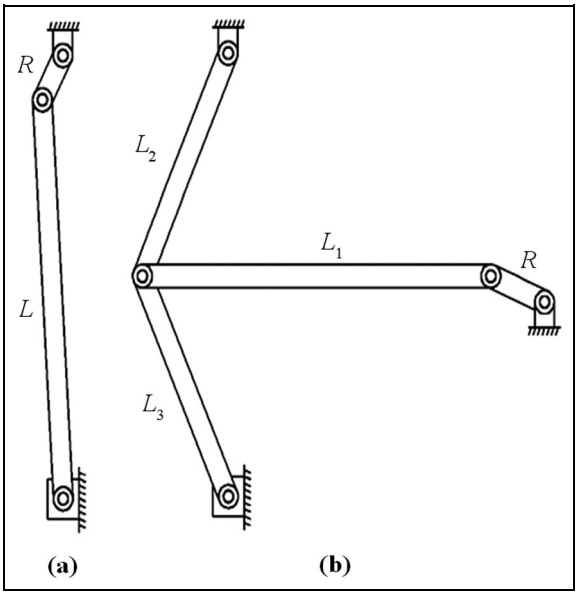

Figure 6. Structure diagrams of the (a) SCM and (b) STM.

Figures 8 and 9 show, respectively, the stroke and speed curves of the slide within one operational period of the three working mechanisms. From Figure 8, it can be seen that when the input crank rotates at a same constant speed, the advance-to return-time ratios of SCM, STM, and SSM are 1.00, 1.06, and 1.67, respectively, indicating that SSM has the best quick-return characteristics. From Figure 9, it can be seen that within nominal pressure stroke (0–6 mm), the average speeds of the slide are 61, 29, and 16 mm/s, implying that the SSM has the best low-speed characteristics.

Table 8. Information about rod length, rod mass, and friction factor of the SCM and STM.

	SCM	STM
Rod length	$R = 100$ mm, $L = 770$ mm	$R = 149$ mm, $L_1 = 1029$ mm, $L_2 = L_3 = 480$ mm
Rod mass	Mass of slide, crank, and connect rod is 500, 150, and 150 kg, respectively	Mass of slide, crank, connect rod, up, and bottom toggle rod is 500, 120, 150, 100, and 100 kg, respectively
Pin radius	Radius of pins in all joints is 85 mm	
Friction factor	Static and dynamic friction factors in all kinematic pairs is 0.05	

SCM: slide-crank mechanism; STM: symmetrical toggle mechanism.

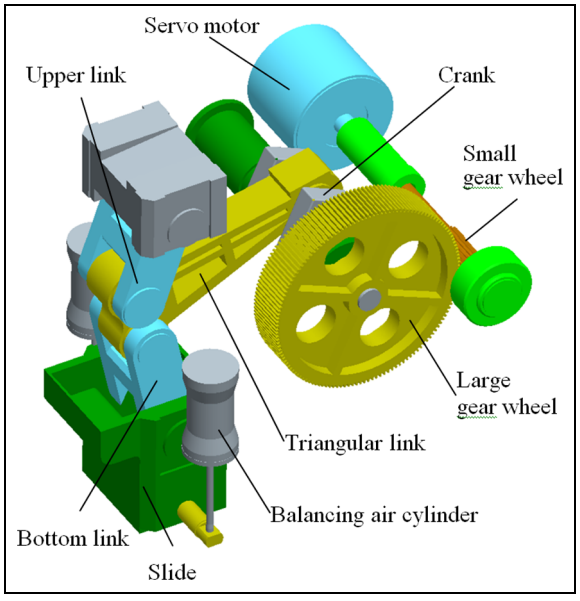

Figure 7. Virtual prototype of the SSM.

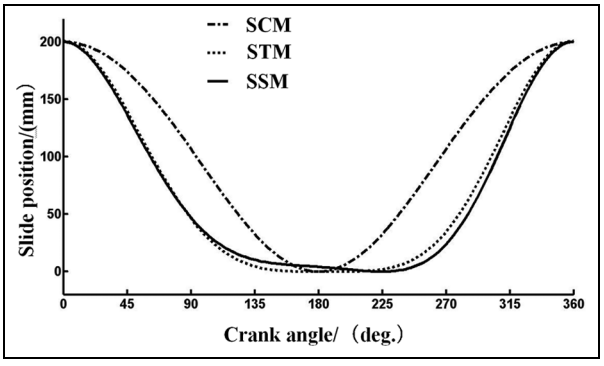

Figure 8. Slide stroke curves.

Figure 10 shows the required crank torques of the three working mechanisms when 4000 kN nominal pressures are applied to the slides within nominal pressure stroke. It can be seen that at 6 mm nominal pressure stroke point, the required crank torque of the SSM is

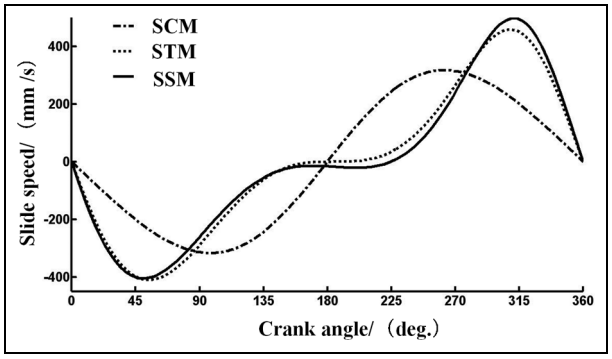

Figure 9. Slide speed curves.

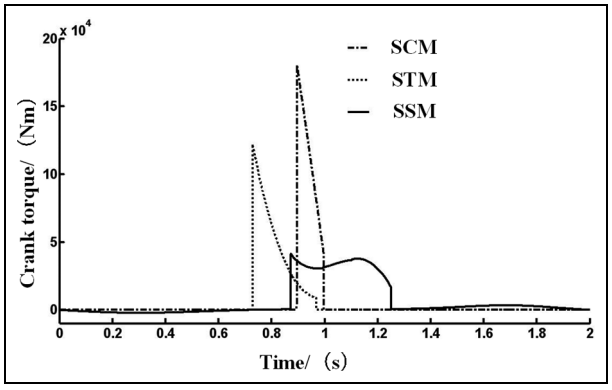

Figure 10. Crank torque curves.

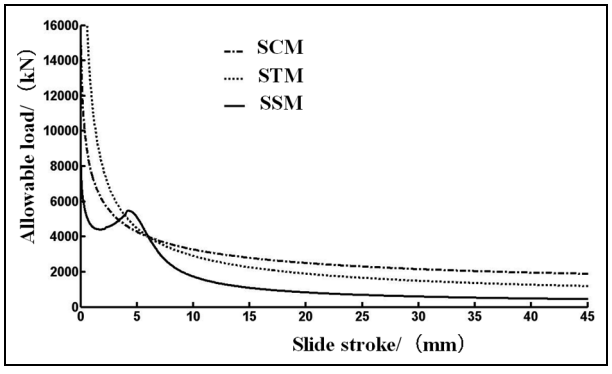

Figure 11. Slide allowable load curves.

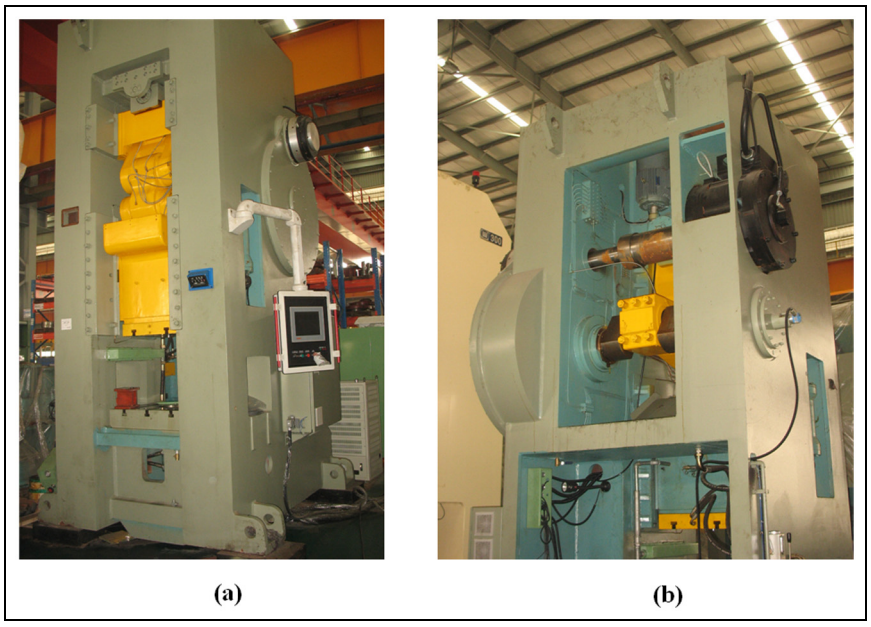

Figure 12. Experimental servo mechanical press with SSM: (a) front side and (b) back side.

41,882 N m, decreasing, respectively, from 180,540 N m by 76.8% and from 122,020 N m by 65.7% when compared with SCM and STM, able to cut down the capacities and costs of servo motors effectively.

Figure 11 shows the allowable loads of the three working mechanisms when the input torque keeps constant within approaching stroke. The allowable load curve is an important performance index and a selection basis for mechanical presses. In order to be convenient for comparison, it is assumed that the nominal pressures at the nominal position (6 mm) of all the three working mechanism are 4000 kN. According to the mechanical advantages of the three working mechanisms, the input torques should be equal to the required torques, namely, 41,882 N m for SSM, 122,020 N m for STM, and 180,540 N m for SCM. It can be seen that when the slide is approaching to the BDC, the allowable load of SSM will decrease first and then increase again, but with a little greater than the nominal pressure 4000 kN.

Experiment validation

In order to validate the transmission characteristics of the designed and optimized Stephenson six-bar working mechanism, an experimental servo mechanical press was designed and manufactured, as shown in Figure 12.

This experimental servo mechanical press was driven by a large capacity servo motor (BAUMULLER, DST2-315, rated power, 78 kW; rated speed, 300 r/min; maximum output torque, 5700 N m), and reduced by a pair of gear wheels (ratio, 1:10). The slide displacement

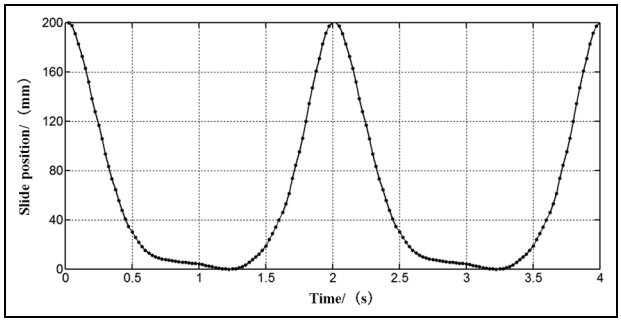

Figure 13. Slide stroke curve of the optimum Stephenson six-bar mechanism by experiment.

can be measured by a grating scale mounted on the slide. The forming force can be applied to the slide by a hydraulic cylinder and was measured indirectly by a pressure transmitter. The driving torque applied to the crank can be measured by a resistance strain gauge with wireless communication function. The forming force and driving torque signals were received synchronously and processed by a dynamic signal analyzer (DonghuaTEST, DH5905). Figure 13 is the slide stroke curve when the servo motor running at a constant angular speed of 300 r/min, which is similar with the simulation curve (shown in Figure 8), with ideal quick-return and dwelling characteristics.

Figure 14 is the comparison of mechanical advantages at different working strokes (within 20 mm) of the three working mechanism, between the simulation and experiment results. It can be seen that in the 6 mm nominal pressure stroke, the mechanical advantage of

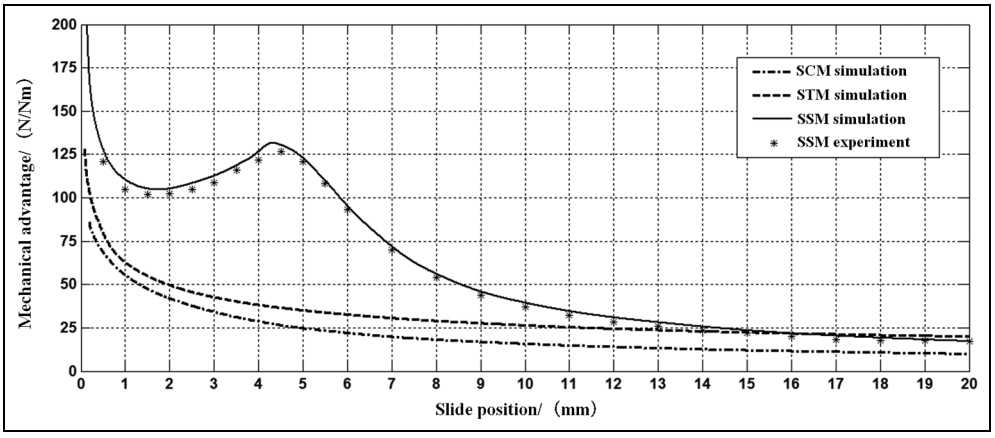

Figure 14. Comparison of mechanical advantages at different working strokes of the three working mechanism between simulation and experiment.

the SSM is apparently higher than that of the STM and SCM. For the former, during the nominal pressure stroke, the mechanical advantage is greater than 100 N/N m, with a rebound to 132 N/N m at 4.3 mm. At the position above the BDC 10 mm, the mechanical advantage is still up to 40 N/N m. And, the experimental results have good agreement with the simulation results.

From the above analysis, it can be validated that the designed and optimized Stephenson six-bar working mechanism has not only high mechanical advantage, but good dwelling characteristics. The higher mechanical advantage makes the SSM cut down greatly the required crank torque, accordingly reducing the required PMSM capacity effectively. The better dwelling characteristics can reduce requirements for varying speed, improving the controllability and saving the energy for acceleration and deceleration.

Conclusion

1. In order to cut down the capacities of the servo motors and reduce the costs of servo mechanical presses, a two-phase, qualitative and quantitative, design scheme of Stephenson six-bar working mechanisms with high mechanical advantage and good dwelling characteristics for servo mechanical presses was proposed.
2. In qualitative design, an instant center analysis method was presented to set up the relationship between mechanical advantage and some special instant centers, and to find the primary mechanism configuration with high mechanical advantage, which is advantageous to reduce the searching domain of design variables and to simplify the numeric computation of optimization model.
3. A sensitivity analysis method is employed to analyze the influences of design parameters to the slide maximum stroke and the slide speed monotonic property, which is useful for the decision of initial and bond values of design variables in optimization.
4. In quantitative design, a multi-objective optimization method, aiming at high mechanical advantage, low-speed characteristics, and slow-moving uniformity, was employed to synthesize the dimensions of the SSM.
5. An experimental servo mechanical press was made, and the tests of slide motion and mechanical advantage were conducted. The experimental results validated the simulation results.
6. Compared with general working mechanisms, the Stephenson six-bar working mechanism has higher mechanical advantage and better dwelling characteristics.

Declaration of conflicting interests

The author(s) declared no potential conflicts of interest with respect to the research, authorship, and/or publication of this article.

Funding

The author(s) disclosed receipt of the following financial support for the research, authorship, and/or publication of this article: This work was supported by 2009 Guangdong-Hong Kong key bidding project (grant number 2009Z21) and Foshan special innovation fund project (grant number 2013AG100063), China.

References

1. Osakada K, Mori K, Altan T, et al. Mechanical servo press technology for metal forming. *CIRP Ann: Manuf Techn* 2008; 60: 1–25.

2. Du R and Guo W-Z. The design of a new metal forming press with controllable mechanism. *J Mech Design* 2003; 125: 82–592.
3. Meng C-F, Zhang C, Lu Y-H, et al. Optimal design and control of a novel press with an extra motor. *Mech Mach Theory* 2004; 39: 11–818.
4. Li H and Zhang Y-P. Seven-bar mechanical press with hybrid-driven mechanism for deep drawing; part 1: kinematics analysis and optimum design. *J Mech Sci Technol* 2010; 24: 2153–2160.
5. Guo W-Z, He K, Yeung K, et al. A new type of controllable mechanical press: motion control and experiment validation. *J Manuf Sci Eng* 2005; 127: 731–742.
6. Ouyang P-R, Li Q, Zhang W-J, et al. Design, modeling and control of a hybrid machine system. *Mechatronics* 2004; 14: 1197–1217.
7. He K, Luo Y-X, Kong C-T, et al. Trajectory planning, optimization and control of a hybrid mechanical press. *WSEAS T Syst* 2009; 8: 614–627.
8. He K, Jin Z-P, Guo W-Z, et al. The design of a new controllable mechanical metal forming press. *Mach Des Res* 2005; 21: 12–14.
9. Tang B-H and Guo W-Z. The new hybrid-driven mechanical presses. *Mach Des Res* 2007; 23: 23–25.
10. Soong R-C. Dynamic analysis of a hybrid-driven 7-bars mechanism. *J Vibroeng* 2014; 16: 945–953.
11. Li H, Zhang Y-P and Zheng H-Q. Dynamics modeling and simulation of a new nine-bar press with hybrid-driven mechanism. *J Mech Sci Technol* 2008; 22: 2436–2444.
12. Tso P-L and Liang K-C. A nine-bar linkage for mechanical forming presses. *Int J Mach Tool Manu* 2002; 42: 139–145.
13. Tokuz L-C and Jones J-R. Programmable modulation of motion using hybrid machine. In: *Eurotech direct'91—IMechE: European engineering research and technology congress*, Birmingham, 2–4 July 1991, paper no. C414/071, pp.85–92. London: Institution of Mechanical Engineers (IMechE).
14. Wang L, Yang J-C and Han X-Q. The performance study of hybrid-driving differential gear trains. *Mod Appl Sci* 2009; 3: 95–102.
15. Guo W-Z and Gao F. Kinematic design of a PKM-type composite actuator. In: *IEEE/ASME international conference on advanced intelligent mechatronics*, Singapore, 14–17 July 2009, pp.1459–1462. New York: IEEE.
16. Guo W-Z and Gao F. Design of a servo mechanical press with redundant actuation. *Chin J Mech Eng* 2009; 22: 574–579.
17. Bai Y-J, Gao F, Guo W-Z, et al. Kinematic and dynamic analyses of the multi-actuated mechanical press with parallel topology. *Proc IMechE, Part C: J Mechanical Engineering Science* 2012; 226: 2573–2588.
18. Sun Y-S, Hu J-G, Zheng H-B, et al. Energy saving drive for forming equipments. *Adv Mat Res* 2011; 154–155: 701–707.
19. Suzuki Y and Hata Y. *Servo press control system and servo press control method*. US7434505B2 Patent, 2008.
20. Norton R-L. *Design of machinery: an introduction to the synthesis and analysis of mechanisms and machines*. Beijing, China: China Machine Press, 2003.
21. Towfigh K. The four-bar linkage as an adjustment mechanism. In: *Proceedings of the applied mechanism conference*, Tulsa, 31 July–1 August 1969, pp.27-1–27-4.
22. Hwang W-M, Hwang Y-C and Chiou S-T. A drag-link drive of mechanical presses for precision drawing. *Int J Mach Tool Manu* 1995; 35: 1425–1433.
23. Chiou S-T, Bai G-J and Chang W-K. Optimum balancing designs of the drag-link drive of mechanical presses for precision cutting. *Int J Mach Tool Manu* 1998; 38: 131–141.
24. Smaili A and Diab N. Optimum synthesis of hybrid-task mechanisms using ant-gradient search method. *Mech Mach Theory* 2007; 42: 115–130.
25. Sun Y-S, Hu J-G, Cheng Y-Q, et al. Characteristics analysis of working mechanisms for servo mechanical presses. *Appl Mech Mater* 2012; 220–223: 762–767.

Appendix 1

Notation

f_i	objective function
F	force
g_i	constraint
I_{ij}	instant center
$\overline{I_{ij}I_{mn}}$	distance between instant center I_{ij} and I_{mn}
$\vec{l}_i$	position vector
MA	mechanical advantage
N	number of sampling data
T	torque
v	linear speed
$\bar{V}$	average value of slide speed within working stroke
V_i	value of slide speed within working stroke
x_i	design parameter
ϕ_{i1}	angle vector
ω	angular speed
ω_i	weighting factor